Available online at www.sciencedirect.com
ScienceDirect
Journal of Solid State Chemistry 181 (2008) 1167–1175
JOURNAL OF SOLID STATE CHEMISTRY
www.elsevier.com/locate/jssc

$IrSr_2TbCu_2O_8$, a high-pressure metamagnetic cuprate: Structure, microstructure and properties

A.J. Dos santos-García[a,1], J. van Duijn[a], R. Saéz-Puche[a], G. Heymann[b], H. Huppertz[b], M.Á. Alario-Franco[a,*]

[a]*Laboratorio de Química del Estado Sólido, Departamento de Química Inorgánica, and Laboratorio Complutense de Altas Presiones, Facultad de Química, Universidad Complutense, 28040 Madrid, Spain (EU)*

[b]*Department Chemie und Biochemie, Ludwig-Maximilians-Universität München, Butenandtstraße 5-13, 81377 München, Germany (EU)*

Received 27 November 2007; received in revised form 15 February 2008; accepted 16 February 2008
Available online 29 February 2008

Abstract

The synthesis, structure and microstructure of the $IrSr_2TbCu_2O_8$ cuprate showing metamagnetic properties are described. The sample was prepared at high temperatures and pressures up to 9.2 GPa. The structure is tetragonal, showing a 1212 type structure, that derives from the classical YBaCuO superconductor structure, replacing the tetracoordinated square planar copper [Cu–O_4] in the "chains" by octahedral [Ir–O_6] groups that form a perovskite-like layer in the basal plane of the unit cell. A "simple" cell, $\sim a_p \times a_p \times 3a_p$, where a_p is the basic perovskite unit cell parameter ($a_p \sim 3.8$ Å), is supported by X-ray powder diffraction (XRD) and a so-called "diagonal" one, $\sim\sqrt{2}a_p \times \sqrt{2}a_p \times 3a_p$, by SAED; a microdomain texture of latter cell and a series of very interesting extended defects have been observed by HREM. Magnetic susceptibility measurements show a magnetic transition, $T_N \sim 6$ K, with negative Weiss temperature, that indicates antiferromagnetic interactions among the Tb moments. The magnetic structure has been determined by neutron diffraction. A detailed magnetic study has revealed a metamagnetic behavior, something not previously observed in this type of cuprates. Specific heat and resistivity measurements have also been performed to characterize the transition.

Keywords: Irido-cuprate; Microstructure; Metamagnetism; 1212 cuprates

1. Introduction

Twenty years ago the discovery of superconductivity in a Ba–La–Cu oxide [1], the first of the now called high temperature superconductors, or HTSC, was the starting point of a new avenue in condensed matter physics and chemistry and, indeed, in materials science. Many new materials have been discovered since which put the superconducting critical temperatures at the, by then unexpected, value of ~136 K at room pressure [2,3] and at the even more impressive 165 K under high pressure [4,5].

Many of the so-called cuprate materials, characterized by the presence of copper–oxygen planes, are indeed superconducting [6] and, although at least as many of them are not so, those can still show interesting properties.

In particular the so-called *M*-1212 family has been the focus of numerous studies, here *M* stands for a number of transition and/or main group elements in a variety of oxidation states and coordination numbers. Indeed, YBaCuO, i.e. $Ba_2YCu_3O_7$, that, in structural terms is better formulated as $CuBa_2YCu_2O_7$, is certainly the prime example. It is still the object of permanent interest for both, the superconducting and the magnetic properties, including the search for applications [7].

This *M*-1212 family is particularly interesting when *M* is ruthenium, namely: $RuSr_2RECu_2O_8$ (*RE*, rare earth cation), first synthesized by Bauerfeind et al. [8,9] since

*Corresponding author. Fax: +34 91 394 4352.
E-mail addresses: antonio.dossantos@pcyta.com (A.J. Dos santos-García), maaf@quim.ucm.es (M.A. Alario-Franco).
[1]Present address: Parque Científico y Tecnológico de Albacete, Instituto de Investigación en Energías Renovables, Universidad de Castilla-La Mancha, Paseo de la Innovación 1, 02006 Albacete, Spain. Fax: +34 967 555 321.

0022-4596/$ - see front matter © 2008 Elsevier Inc. All rights reserved.
doi:10.1016/j.jssc.2008.02.022

there was a continuous debate in the literature to confirm/disprove whether it is a material where superconductivity and magnetism do coexist. These two important properties have been reputed to be antagonic [10–15]. Obviously, with this interesting behavior, a number of studies have been performed to substitute ruthenium by other elements, in order to modify both the magnetic and the superconducting properties.

In fact, more than twenty partial substitutions of the Ru [16–20], Sr [21] and Cu [22,23] atoms have been performed; only tin [18] and copper [19], in the place of ruthenium seem to have a positive effect and both show an increase of T_C from 36 to 42 and 70 K, respectively. At the same time, T_N seems to decrease in both cases, something that is attributed to the disorder introduced in the ruthenium sublattice by the dopants. Replacing the rare earth has also been an interesting source of new materials and properties [24,25]. Yet, for the majority of the rare earth elements (all except Eu, Sm, and Gd) high pressure is required to achieve the substitution. In this way, it was found that the Y member, namely $RuSr_2YCu_2O_8$, exhibits the highest critical temperature of the family [25] ($T_C = 51$ K) (see also Akimitsu [26]).

Recently, a series of non-superconducting phases with the general formula $CrSr_2RECu_2O_8$ [12] were obtained using high pressure and temperature techniques. An antiferromagnetic ordering is present in some of these chromates when *RE* is a non-magnetic lanthanide, while the rest of the materials seem to exhibit a paramagnetic behavior.

We have, of late, started a project to replace ruthenium by iridium [27]. Here we found that the non-superconducting Gd case, i.e. $IrSr_2GdCu_2O_8$, is ferrimagnetic, the first *M*-1212 cuprate with this feature. Continuing along this route, we present in here the case of $IrSr_2TbCu_2O_8$ which, although non-superconducting, seems to be the first example showing metamagnetism in the *M*-1212 family. A detailed study of this material is reported.

2. Experimental

The sample was prepared, as previously reported for ruthenates [24], chromates [12,24] and iridates [27], in a two-step process. The first one corresponds to the preparation of a mixed Sr–Cu oxide of adequate stoichiometry according to:

$$SrCO_3 + CuO \rightarrow SrCuO_2 + CO_2, \quad (1)$$

by heating in air for two days at 1323 K. In a second step, this precursor was mixed with the appropriate amounts of Tb_4O_7 and IrO_2 oxides (AR, Sigma-Aldrich) loaded in air within a BN crucible and treated in a Walker-type multianvil pressure module [28,29] (installed at the Ludwig-Maximilians-Universität München), according to:

$$2\,SrCuO_2 + \tfrac{1}{4}Tb_4O_7 + IrO_2 + \tfrac{1}{4}O_2 \rightarrow IrSr_2TbCu_2O_8, \quad (2)$$

in which oxygen is taken from the atmosphere [12,24,27]. The typical reaction path was as follows: (i) increasing the pressure up to 9.2 GPa, (ii) rising the temperature up to 1373–1473 K in 15 min, (iii) maintaining there for 20 min, and (iv) quenching to room temperature. Afterwards, the pressure was decreased to ambient conditions in 9 h.

The sample was characterized by X-ray powder diffraction (XRD) performed in a Philips X'Celerator diffractometer (Cu$K\alpha$1-radiation, $\lambda = 1.54056$ Å). The XRD pattern was refined with the Rietveld procedure using the Fullprof_Suite program [30].

Sample composition was checked by EDS (Link Pentafet 5947 Model, Oxford Microanalysis Group) in a transmission electron microscope (TEM) (Jeol JEM FX2000) by in situ observations. High-resolution TEM images and SAED were performed on a Jeol JEM 3000EX microscope.

Magnetic susceptibility measurements were performed at different magnetic fields strengths over the temperature range 1.9–300 K, using a SQUID Quantum Design XL-MPMS magnetometer in zero field cooling (ZFC) and field cooling (FC) conditions. Hysteresis loops, specific heat, and resistivity measurements were performed using a Quantum Design PPMS. The resistivity measurement was done on a pellet according to the Van der Pauw method [31,32]. The temperature ranged from 1.9 to 300 K using magnetic fields up to 9 T.

Neutron diffraction data were collected at 1.8, 15, and 40 K using the D20 diffractometer at the Institute Laue Langevin, Grenoble, France. Fifty milligrams of $IrSr_2TbCu_2O_8$ were placed in a sealed vanadium can ($\varnothing = 4.8$ mm) within a He cryostat. The diffraction profiles were collected in the range $2\theta = 0$–160° with a neutron wavelength of 1.3 Å. The counting times at each temperature were 320, 230, and 390 min, respectively. Rietveld analysis of the profiles was carried out using the Fullprof_Suite program [30].

3. Results and discussion

3.1. Structure

The Rietveld refinement of the XRD data (Fig. 1) indicates that the average crystal structure of the $IrSr_2TbCu_2O_8$ is tetragonal (space group: *P*4/*mmm*) with the parameters $a = 3.8488(1)$ Å, $c = 11.5808(4)$ Å, and $V = 171.552(8)$ Å^3. These values are in good agreement with those obtained from the ruthenates [24,33], chromates [12], and other iridates [27]. As often observed in H.P. samples of multi-cationic materials, some of the minor impurities detected were identified as $(Sr_2Tb)(Cu_2Ir)O_{3-\delta}$ and Cu_2O. These were taken into account in both the refinement and magnetic properties.

Table 1 shows the refined atomic parameters and agreement factors for $IrSr_2TbCu_2O_8$. We took into account the observed splitting in the O(1) and O(3) positions present in this structure [33]; the atomic thermal displacements, U_{iso}, corresponding to all atoms were fixed. Due to the relatively weak scattering factor of oxygen, compared

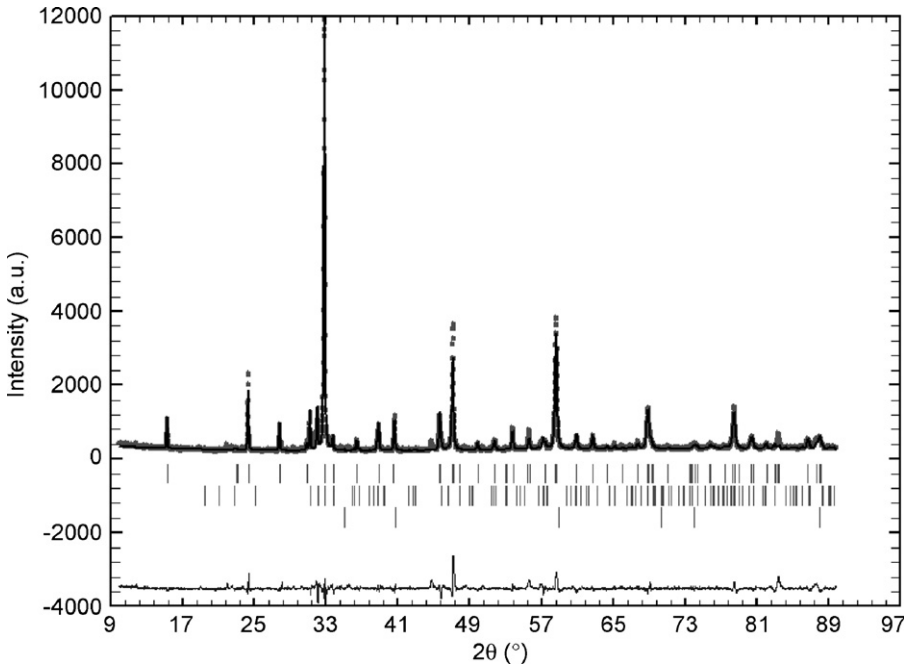

Fig. 1. Rietveld refinement of the X-ray powder diffraction data of $IrSr_2TbCu_2O_8$ (first row of ticks). Impurities taken into account are $(Sr_2Tb)(Cu_2Ir)O_{3-\delta}$ (second row) and a small amount of the high pressure phase Cu_2O (third row). The arrow indicates a reflection from the stainless steel sample holder.

Table 1
Refined cell and atomic parameters and agreement factors for the $IrSr_2TbCu_2O_8$ compound

Space group	a (Å)	c (Å)	V (Å^3)	R_{wp}	R_F	χ^2
*P*4/*mmm* (1 2 3)	3.8488 (1)	11.5808(4)	171.552(8)	0.108	0.059	4.38
Atom	Wyckoff position	x	y	z	$B_{overall}$	Occ
Ir	1 (*a*)	0	0	0	1.39(6)	1.0
Sr	2 (*h*)	0.5	0.5	0.1958(4)	1.39(6)	1.0
Tb	1 (*d*)	0.5	0.5	0.5	1.39(6)	1.0
Cu	2 (*g*)	0	0	0.3610(5)	1.39(6)	1.0
O(1)	4 (*n*)	0.123(7)	0.5	0	1.39(6)	0.25
O(2)	4 (*i*)	0.5	0	0.379(1)	1.39(6)	1.0
O(3)	2 (*g*)	0	0	0.139(2)	1.39(6)	0.5

to heavy atoms such as Sr and Ir, only the overall thermal displacement parameters were refined. This new material is, then, isostructural with the gadolinium iridate and indeed shows a 1212 type structure (Fig. 2).

3.2. Microstructure

The microstructure of this new cuprate, see below, matches nicely with the microdomain texture previously observed in 1212 type compounds [27,33]. The metallic compositions of the main phase and of the impurities were confirmed by EDS.

Electron microscopy and diffraction suggest the existence of a structurally more complex situation and gives a detailed view of the real structure. The material shows an interesting three-dimensional microdomain texture. In the electron diffraction pattern, shown in Fig. 3, the strong spots can be indexed on the basis of a $[0\,0\,1]_p$ zone axis,

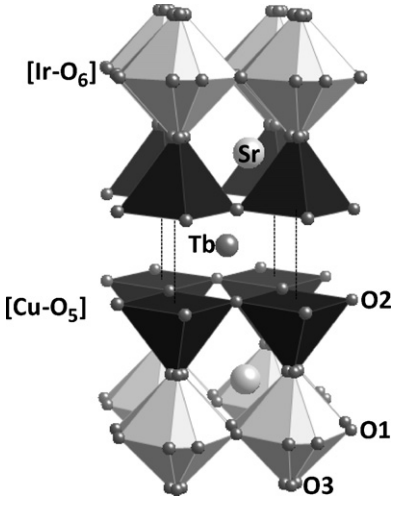

Fig. 2. Crystal structure of $IrSr_2TbCu_2O_8$. Ir sits at the octahedra while copper resides in the square pyramids. The sequence of *A*-cations along the *c*-axis is Sr–Tb–Sr.

where the sub-index p refers to the basic perovskite structure. Besides, some weak spots at $h/2\,k/2\,0$, where h and k are integers, suggest the presence of the well known "diagonal cell", $\sim a_p\sqrt{2} \times a_p\sqrt{2} \times 3a_p$, common in some perovskite structures or superstructures, such as $CaTiO_3$ itself [34,35]. This superstructure is due to the tilt of the octahedra. There are also spots at $h/3\,0\,0$ and $2h/3\,0\,0$ as well as spots at $0\,k/3\,0$ and $0\,2k/3\,0$, that treble the a and b perovskite axes, respectively; this is a clear indication of the presence of a microdomain texture [36–38]. In the light of this, the crystal is then formed by three subsets of domains in which the unit cell is $\sim a_p\sqrt{2} \times a_p\sqrt{2} \times 3a_p$ and the long $3a_p$ c-axis (which is due to the Sr–Tb–Sr ordered sequence along c, Fig. 2) is oriented, in each set, along one of the three space directions.

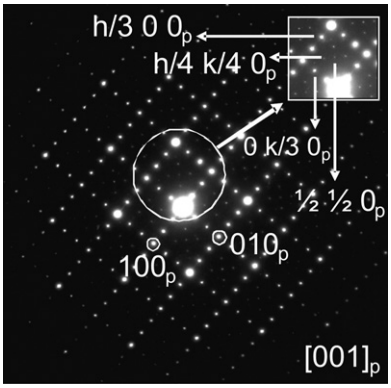

Fig. 3. Electron diffraction pattern of a typical crystal of $IrSr_2TbCu_2O_8$ along the $[0\,0\,1]_p$ zone axis. Besides the strong spots characteristic of the perovskite type subcell, there are a number of other spots. For explanation see text.

There are still some weak extra reflections, located at $h/4\,k/4\,0$ (h and k: integers), which can be attributed to multiple diffraction due to the presence of domain walls. It is interesting to note that there is no evidence of an orthorhombic distortion in any of the ED patterns obtained. Nor have we seen a doubling of the tetragonal c_t axis as observed by Lebedev et al. in some thin films of the isostructural $RuSr_2GdCu_2O_8$ compound [39–41].

This somewhat complicated diffraction information can be properly understood with the aid of the corresponding electron micrographs shown in Figs. 4a and 5a. In Fig. 4a, microdomains are present in which the long c_t-axis ($\sim 3a_p$) alternates at random in one of the three space directions

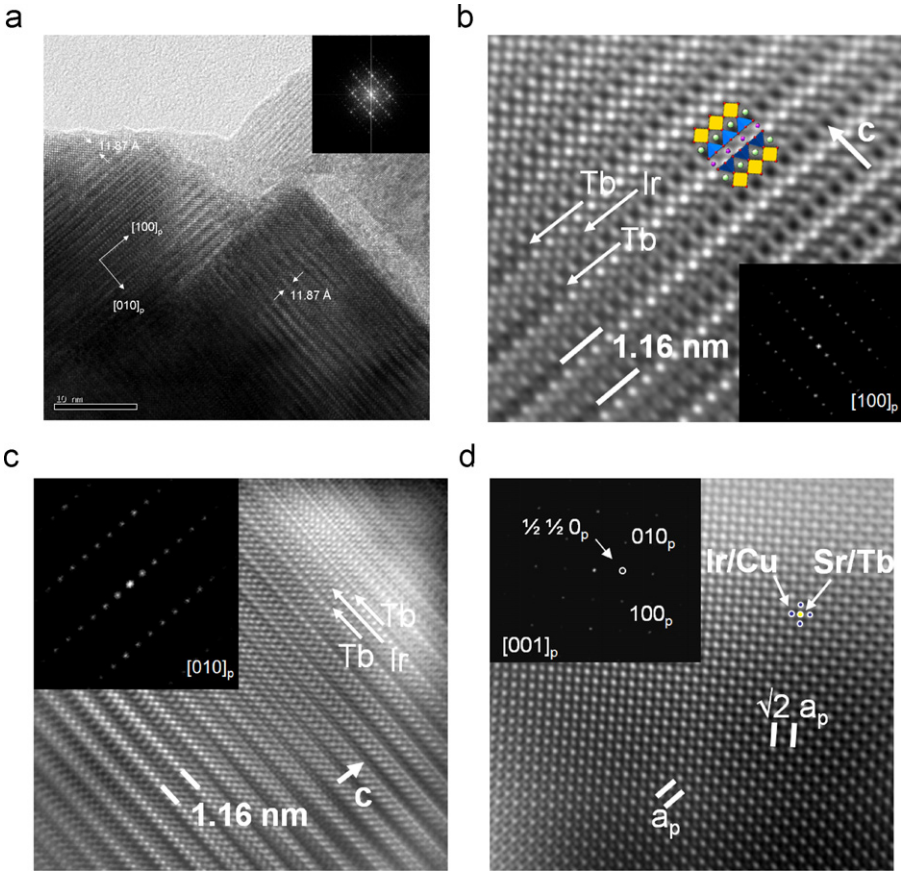

Fig. 4. (a) TEM micrograph of a typical $IrSr_2TbCu_2O_8$ crystal showing a domain structure. Inset shows the Fourier transform of the image. It is similar to Fig. 3 except for the absence of twin-related spots. (b) Part of image on Fig. 4a reconstructed by using reflections from the first domain set $a_p\sqrt{2} \times a_p\sqrt{2} \times 3a_p$ along $[1\,0\,0]_p$ $[1\text{–}10]_t$. Subindex p indicates the perovskite subcell; subindex t indicates the tetragonal superstructure. (c) Part of image on Fig. 4a reconstructed by using reflections from the second domain set $a_p\sqrt{2} \times 3a_p \times a_p\sqrt{2}$ along $[0\,1\,0]_p$ $[1\,1\,0]_t$. (d) Part of image on Fig. 4a reconstructed by using reflections from the third domain set $3a_p \times a_p\sqrt{2} \times a_p\sqrt{2}$ along $[0\,0\,1]_p$ $[0\,0\,1]_t$.

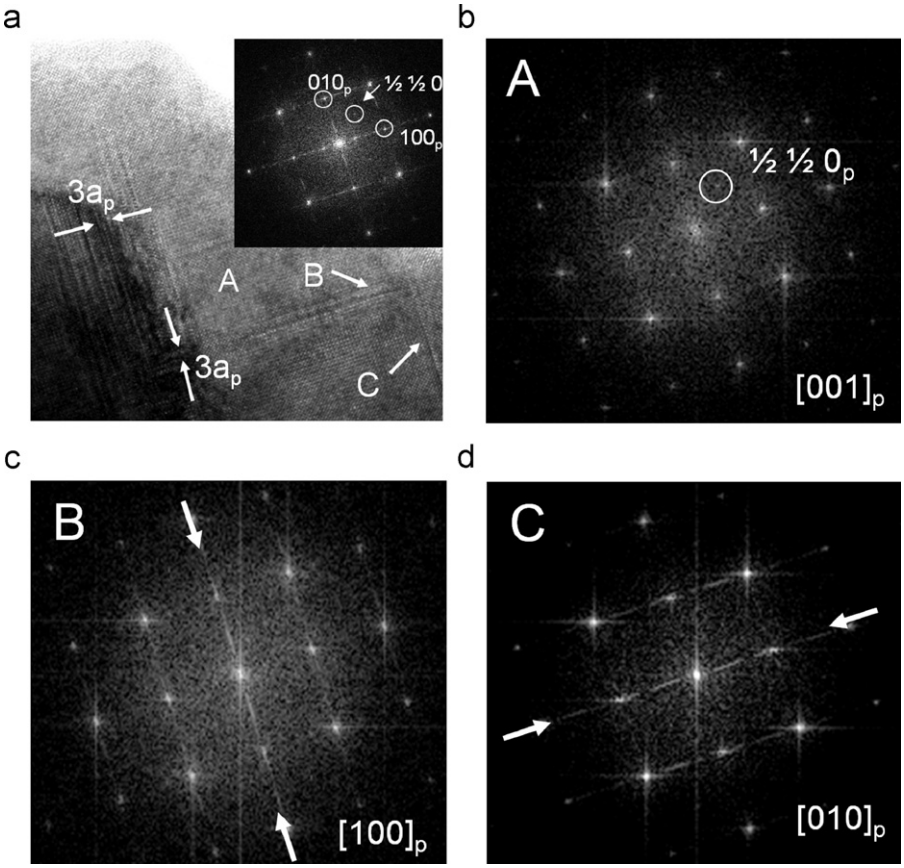

Fig. 5. (a) TEM micrograph of another—less frequent-type of crystal of $IrSr_2TbCu_2O_8$. Two domain sets, *B* and *C*, are only extended at the unit cell level in one dimension (their *c*-axis): i.e. they are to be considered as extended defects. The third domain, *c*-vertical, predominates. (b) Fourier transform of region *A*. (c) Fourier transform of region *B*, streaking along 010_p arrows is due to the presence of an isolated extended defects. (d) Fourier transform of region *C*, streaking along 100_p arrows is due to the presence of an isolated defects perpendicular to the one shown in Fig. 5c. Adding up Fig. 5b–d, gives the pattern shown as an inset on Fig. 5a.

(i.e. $\sim a_p\sqrt{2} \times a_p\sqrt{2} \times 3a_p$ and circular permutation). The Fourier transform of the entire area of the image is shown in the inset of Fig. 4a, and it obviously coincides with the observed electron diffraction pattern. By using the Fourier transform of the entire area, using the Digital Micrograph 3.8.2-Gatan software, we can reconstruct the image of the three different domains: in this mode, Fig. 4b and c show the reconstructed images selecting only the $(h/3\,0\,0)_p$ and $(0\,k\,0)_p$ maxima and $(0\,k/3\,0)_p$ and $(h\,0\,0)_p$ maxima, respectively. They show the structure of the domains seen in Fig. 4a. An image of the unit cell is included for comparison. The third set of domains can be obtained by selecting the spots at $(h/2\,k/2\,0)_p$ corresponding specifically to the diagonal cell, along the c_t axis. The corresponding reconstructed image, Fig. 4d, clearly shows the indicated cell down the $(0\,0\,1)_p$ direction.

Not all crystals studied showed such a clear picture of the microdomain texture: Fig. 5a shows an example of a less common but very interesting situation. In it, dispersed in a wide region, the $a_p\sqrt{2} \times a_p\sqrt{2} \times 3a_p$ cell, with c_t vertical, predominates and portions of the other two orientations of $IrSr_2TbCu_2O_8$ *one unit cell thick* along their *c*-axis and "infinite" (~200 Å) along the *a* and *b* directions are intergrown. These "small pieces" of the main structure in different orientations are in fact to be considered as *extended defects* [42,43]. The Fourier transform of the whole crystal, inset in Fig. 5a, can be decomposed in three diagrams, each one corresponding to three different regions, Figs. 5b–d. Fig. 5b, corresponding to the more abundant domain, represents a "normal" diagram, i.e. with the intensities corresponding to the $[0\,0\,1]_p$ zone axis including the $(h/2\,k/2\,0)$ reflections. As the presence of the domains with $c_t = 3a_p$ in this crystal is so limited, the FFT does not show a well formed superstructure as in Fig. 4a; just streaking along 100_p or 010_p, Fig. 5c and d, can be observed. It is to be stressed that the simple presence of a single extended defect originates streaking in the diffraction pattern or the FFT of the image [42,43]. The presence of this unusual microstructure, in which single extended defects are present embedded in a full matrix of the "normal" phase, is quite novel and interesting in this type of compounds.

This particular texture is due to a lack of equilibrium in the high-pressure synthesis. Some crystals show extended defects containing a simple unit cell of the main structure distributed at random, though at perpendicular directions, as occurs within the domains. As for the presence of 3D-microdomains, instead of a normal crystal, it seems to be

due to the synthesis conditions. If the crystal starts to grow from a high temperature situation there is, in principle, the same choice for it to grow from any point of the mass of the solid; and, from there, it can actually grow in any of the three space directions. These growing fronts then coalesce to give the microdomain texture. Yet the size of the domains is very much dependent on annealing/quenching conditions [38] most likely due to the relative importance of the nucleation/growth process. As for the domain boundaries, they can be planar and give extra spots as in Fig. 3 or more heterogeneous, in which case no supplementary spots are observed on the ED pattern as in the inset of Fig. 4a. However, not all perovskite superstructures show these types of microdomains; their presence seems to be closely related to the amount of distortion from cubic symmetry of the corresponding subcell; see reference [36] for details.

In summary we can conclude that the microstructure of $IrSr_2TbCu_2O_8$ is characterized by a so-called "diagonal" cell, $\sim a_p\sqrt{2}\times a_p\sqrt{2}\times 3a_p$, distributed in 3D domain sets, as supported by SAED and HREM, while a "simple" cell $a_p\times a_p\times 3a_p$ is the only one seen by XRD. This is a consequence of the longer coherence length required in X-ray diffraction as compared with electron diffraction [44].

3.3. Magnetic and electric properties

The magnetic susceptibility data obtained from a pellet of $IrSr_2TbCu_2O_8$ (Fig. 6) follows a Curie–Weiss behavior over a wide range of temperatures, and shows a pronounced maximum at approximately 6 K. Note that in Cu_2O, one of the observed impurities, the copper oxidation state is Cu^{1+} with an electronic configuration $[Ar]3d^{10}$; therefore, a non-magnetic behavior is to be expected for this compound [45,46]. The second impurity, $(Sr_2Tb)(Cu_2Ir)O_{3-\delta}$, however, corresponds to a new single perovskite type phase [47]. Considering the ABO_3 notation, the Sr and Tb cations randomly occupy in such compound the A perovskite position while the Cu and Ir atoms are placed in the B positions [47]. Susceptibility measurements performed on these new disordered phases (reference [47] and work in progress), $(Sr_2RE)(Cu_2Ir)O_{3-\delta}$ with RE = Nd, Sm, Eu, Gd, and Tb, clearly suggest paramagnetic behavior in all cases. We can therefore conclude that the maximum observed in the susceptibility arises from the main sample.

From the corresponding reciprocal susceptibility plot, see inset on Fig. 6, the experimental magnetic moment takes the value of 9.7 μ_B, which agrees very well with the theoretical Tb^{3+} ($^7F_6$) one, ~9.72 μ_B. Taking into account the negative Weiss temperature, −22.73 K, it is reasonable to assign the maximum centered at ~6 K to an AFM ordering transition.

However, a more detailed study of the magnetic and electric properties of this new oxide shows a more complex situation, which can be associated with metamagnetism. This relatively uncommon but very interesting phenomenon has been observed in, for example, some Ruddlesden-Popper phases such as $Sr_3Ru_2O_7$ [48–50], some oxysulfides [51], and even in *simple* $FeCl_2$ [52]. Although metamagnetism has been observed in a Ru-1222 compound [53], it has not been observed so far in the M-1212 family of cuprates.

In Fig. 7 one can see the magnetization of a pellet of $IrSr_2TbCu_2O_8$ for applied magnetic fields up to 5 T at different temperatures. Metamagnetism is clearly seen in the 2 and 7 K data, which cross at a critical field of 2 T. This is even more obvious in the first derivative of the magnetization versus field plot, shown in the inset. As metamagnetism is associated in insulators or metals with different mechanisms resistivity (ρ) measurements were performed in order to clarify the electric nature of the $IrSr_2TbCu_2O_8$ material.

In the Log ρ versus $1/T$ plot shown in Fig. 8, one can see that the resistivity clearly decreases as temperature increases: a semiconducting behavior is apparent. Yet,

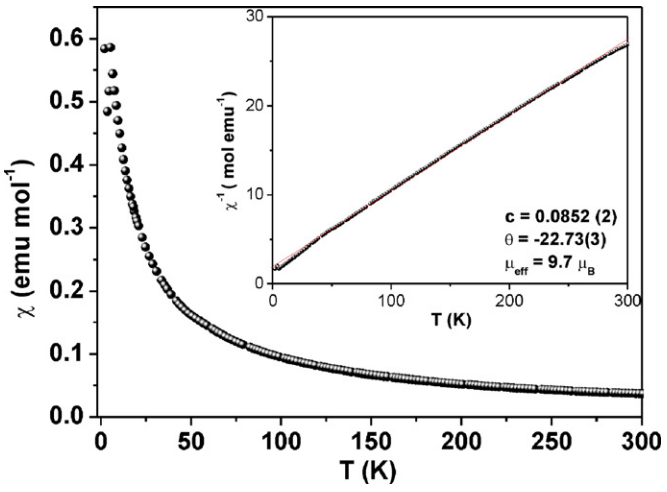

Fig. 6. Magnetic susceptibility as a function of temperature. The inset shows Curie–Weiss behavior.

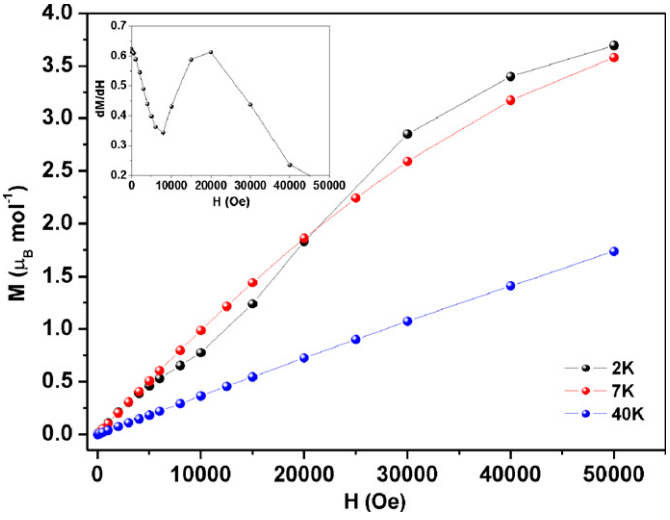

Fig. 7. M versus H at different temperatures. The crossing of the top curves is indicative of metamagnetism. Inset shows the first derivative of the magnetization versus H at 2K.

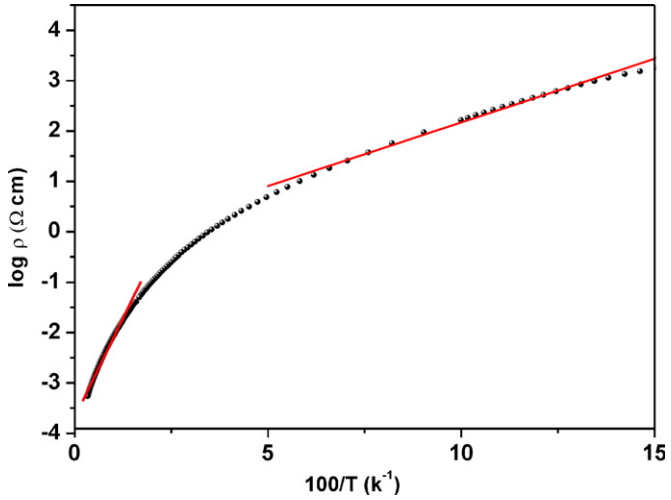

Fig. 8. Log resistivity versus reciprocal temperature. Two rather different slopes are seen in the two temperature regions covered by the visual aid tangents to the plot.

although no obvious signature of a M/I transition can be discerned, two rather different slopes are seen in the two temperature regions covered by the visual aid tangents to the plot. The corresponding activation energies for conduction are 0.0136 eV and 2.18×10^{-3} eV, respectively. This is an indication of the greater electron localization at low temperature. This increase in resistivity can be attributed to incipient magnetic interactions. Close to the Neel temperature the beginning of magnetic moment ordering results in a large increase in the resistivity due to the localization of the electrons in the magnetic ordered state. Consequently, the metamagnetic state is obviously insulating.

On the other hand, in $IrSr_2TbCu_2O_8$, the metamagnetism seems to be associated with a spin–flop transition. For a spin–flop transition, saturation of the magnetization would be reached at 2 T, where the crossing of the magnetization versus field plots at 2 and 7 K is observed. As this is not the case, we favor a spin–flop transition. Moreover, Fig. 7 shows that saturation is not reached even at 5 T. In fact, up to 9 T saturation was not achieved (data not shown).

In order to obtain more quantitative information about the magnetic transition, specific heat measurements were performed as a function of temperature at different magnetic field strengths. Fig. 9 shows the presence of a λ-type transition at ~4.6 K (see inset) in the absence of a field, which corresponds to the AFM ordering observed at about the same temperature in the magnetic susceptibility data (Fig. 6). As the external magnetic field is progressively increased up to 9 T, one can see the concomitant vanishing of the λ-type transition (Fig. 10) and a slight displacement of the transition temperature to lower values. It is quite clear that, as the magnetic field increases, the magnetic ordering is progressively destroyed and, consequently, the specific heat decreases. As a result the material becomes paramagnetic. This confirms that the transition at T_N is to

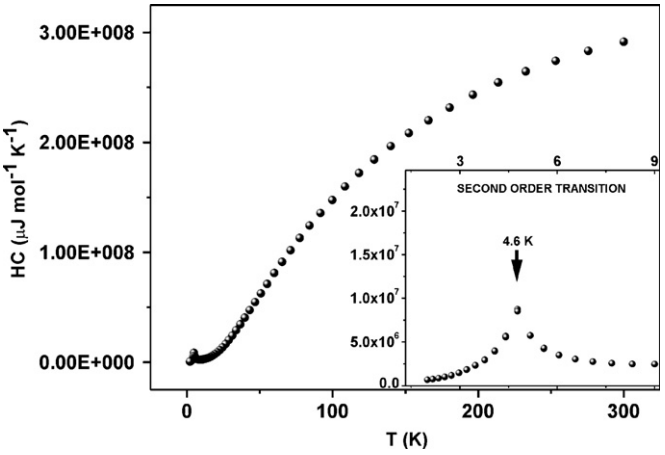

Fig. 9. Heat capacity as a function of temperature showing the transition.

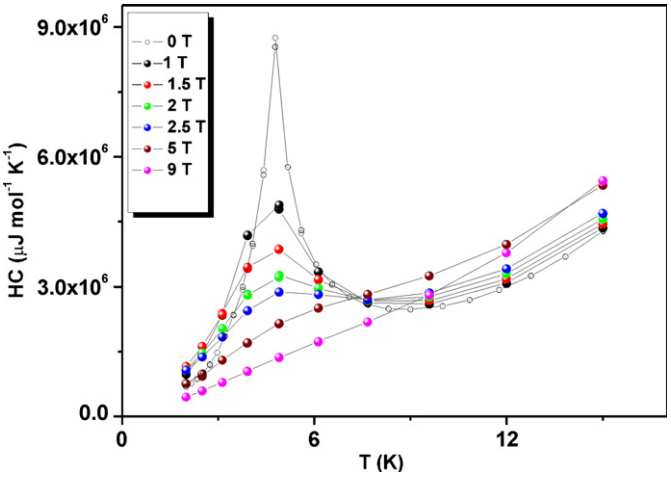

Fig. 10. Influence of magnetic field in heat capacity. The heat of the transition progressively decreases as the field increases.

an AFM ordered state as in the case of FM ordering an increase in the specific heat would be observed [54]. In this respect it is worth mentioning the AFM-like hysteresis loop observed at 2 K, Fig. 11.

3.4. Magnetic structure determination

The difference between the profiles collected at 1.8 (below T_N) and 40 K (well above T_N) profiles is shown in Fig. 12. Magnetic reflections are clearly observed in the difference data, confirming a magnetic transition at T_N to a long range ordered state. Assuming the $\sqrt{2}a_p \times \sqrt{2}a_p \times 3a_p$ structural unit cell, these reflections can be indexed by the $(0\,0\,\frac{1}{2})$ propagation vector. The intensities are fitted by a two sublattice model with moments parallel to the c-axis. The moments are coupled antiferromagnetically to their nearest-neighbors in the [1 1 0] and [0 0 1] directions (see inset in Fig. 12). This is consistent with the observed negative Weiss temperature. Due to the poor statistics for the fit shown in Fig. 12 the size of the Tb moments were fixed to that obtained from our susceptibility measurements (i.e. 9.7 μ_B).

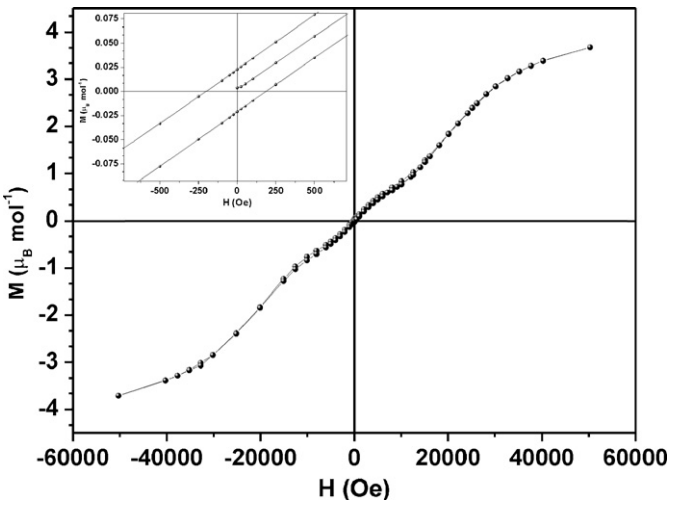

Fig. 11. Isothermal magnetization curve at 2 K. Note the AFM-like-shape hysteresis loop.

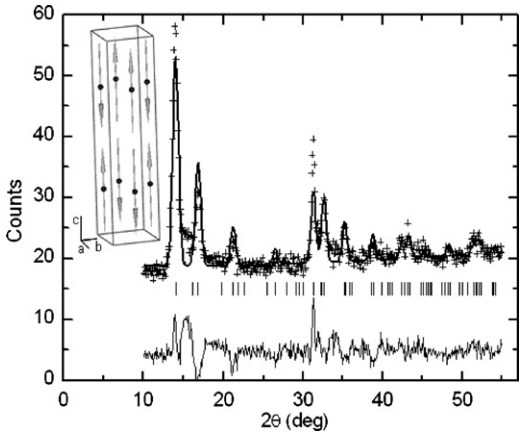

Fig. 12. Magnetic structure fit from the difference between the 1.8 and 40 K D20 neutron diffraction profiles of $IrSr_2TbCu_2O_8$. Crosses, upper and lower solid line show observed, calculated and difference patterns, respectively. Ticks only correspond to the magnetic structure. Inset shows the schematic representation of the magnetic structure in $IrSr_2TbCu_2O_8$ at 1.8 K.

4. Conclusions

We have prepared, at rather high pressure (9.2 GPa) and high temperature (~1400 K) a new *M*-1212 type cuprate, $IrSr_2TbCu_2O_8$ which, although non-superconducting, shows a very interesting set of properties. Among them, one can mention its crystal structure, where some of the oxygens show split positions as well as a very interesting microstructure characterized by three-dimensional micro-domains of different sizes. We have also determined the magnetic structure and explained the rather unusual magnetic properties, which correspond to metamagnetic behavior in an insulating state. This is, to our knowledge, the first example of metamagnetism in the already numerous *M*-1212 type cuprates. These interesting magnetic properties are very different from those of the homologous Gd–cuprate, which, as we have shown recently, is ferrimagnetic [27]. As usually happens in this type of compounds, the Cu sublattice is ordered antiferromagnetically at high temperatures while, for obvious reasons the Ir^{5+} ions do not contribute to the magnetic interactions.

Acknowledgments

We would like to thank financial support from CICYT, programa MAT2004-01641, Comunidad Autonoma de Madrid, programa MATERYENER, PRICYT S-0505/PPQ-0093 (2006), Fundación Areces, Programa Física de Bajas Temperaturas (2003), the European Science Foundation within the COST D30 network (D30/003/03) and the Ramon y Cajal program (RYC-2005-001064). We also thank Dr. J. Romero de Paz for technical assistance and E. Castillo-Martinez and A. M. Arévalo-López for the effort put in the determination of the specific heat and resistivity measurements. Authors also want to thank Dr. Vincent Legrand (ILL) for help in collecting the neutron powder pattern.

References

[1] A.K. Muller, G. Bednorz, Z. Phys. B 64 (1986) 189.
[2] S.N. Putilin, E.V. Antipov, M. Marezio, Physica C 212 (1993) 226.
[3] A. Schilling, M. Cantoni, J.D. Guo, H.R. Ott, Nature 363 (1993) 56.
[4] M. Nuñez-Regueiro, J.L. Tholence, E. Antipov, J.J. Caponi, M. Marezio, Science 262 (1993) 97.
[5] C.W. Chu, L. Gao, F. Chen, Z.J. Huan, R.L. Meng, Y.Y. Xue, Nature 365 (1993) 323.
[6] C.P. Poole Jr., H.A. Farach, R.J. Creswick, in: C.P. Poole (Ed.), Handbook of Superconductivity, vol. 1, Academic Press, San Diego, 2000, pp. 1–693.
[7] J. Figueras, T. Puig, X. Obradors, W.K. Kwok, L. Paulius, G.W. Crabtree, G. Deutscher, Nat. Phys. 2 (6) (2006) 402.
[8] L. Bauernfeind, W. Widder, H.D. Braun, Physica C 254 (1995) 151.
[9] L. Bauernfeind, W. Widder, H.D. Braun, J. Low Temp. Phys. 105 (1996) 1605.
[10] L. Ginzburg, Zh. Exsp. Teor. Fiz. 31 (1956) 202.
[11] M.B. Maple, Physica B 215 (1995) 110.
[12] R. Ruiz-Bustos, M.H. Aguirre, M.Á. Alario-Franco, Inorg. Chem. 44 (2005) 3063.
[13] J.W. Lynn, B. Keimer, C. Ulrich, C. Bernhard, J.L. Tallon, Phys. Rev. B 61 (2000) R14964.
[14] I. Dzyzloshinsky, J. Phys. Chem. Solids 4 (1958) 241.
[15] T. Moriya, Phys. Rev. 120 (1960) 91.
[16] A. Hassen, J. Hemberger, A. Loidl, A. Krimel, Physica C 400 (2003) 71.
[17] S. Malo, D. Ko, J.T. Rijssenbeek, A. Maignan, D. Pelloquin, V.P. Dravid, K.R. Poeppelmeier, Int. J. Inorg. Mater. 2 (2000) 601.
[18] A.C. McLaughlin, J.P. Attfield, Phys. Rev. B 60 (1999) 14605.
[19] P.W. Klamut, B. Dabrowski, S. Kolesnik, M. Maxwell, J. Mais, Phys. Rev. B 63 (2001) 224512.
[20] M.S. Torikachvili, I. Bossi, J.R. O'Brien, F.C. Fonseca, R. Muccillo, R.F. Jardim, Physica C 408–410 (2004) 195.
[21] P. Mandal, A. Hassen, J. Hemberger, A.A. Krimmel, A. Loidl, Phys. Rev. B 65 (2002) 144506.
[22] J.L. Tallon, J.W. Loram, G.V.M. Williams, C. Bernhard, Phys. Rev. B 61 (2000) R6471.
[23] J.E. McCrone, J.L. Tallon, J.R. Cooper, A.C. McLaughlin, J.P. Attfield, C. Bernhard, Phys. Rev. B 68 (2003) 064514.

[24] R. Ruiz-Bustos, Ph.D. Thesis, Universidad Complutense, Madrid, Spain, 2003.
[25] R. Ruiz-Bustos, J.M. Gallardo-Amores, E. Morán, V. García-Baonza, M.Á. Alario-Franco, High Press. Res. 22 (2002) 573.
[26] Y. Tokunaga, H. Kotegawa, K. Ishida, Y. Kitaoka, H. Takagiwa, J. Akimitsu, Phys. Rev. Lett. 86 (2001) 5767.
[27] A.J. Dos santos-García, M.H. Aguirre, E. Morán, R. Saéz-Puche, M.Á. Alario-Franco, J. Solid State Chem. 179 (2006) 1296.
[28] D. Walker, M.A. Carpenter, C.M. Hitch, Am. Mineral. 75 (1990) 1020.
[29] H. Huppertz, Z. Kristallogr. 219 (2004) 330.
[30] J. Rodriguez-Carvajal, Physica B 192 (1993) 55.
[31] L.J. Van der Pauw, Philips Res. Rep. 13 (1953) 1.
[32] L.J. Van der Pauw, Philips Res. Rep. 20 (1958/59) 220.
[33] M.H. Aguirre, R. Ruiz-Bustos, M.Á. Alario-Franco, J. Mater. Chem. 13 (5) (2003) 1156.
[34] R.H. Mitchell, in: R.H. Mitchell (Ed.), Perovskites: Modern and Ancient, vol. 1, Almaz Press, Ont., 2002, p. 2 (Chapter 1).
[35] H.F. Kay, P.C. Bailey, Acta Cryst. 10 (1957) 219.
[36] A. Vegas, M. Vallet-Regí, J. Gonzalez-Calbet, M.Á. Alario-Franco, Acta Cryst. B 42 (1986) 167.
[37] M.Á. Alario-Franco, M.J. Henche, M. Vallet, J. Gonzalez-Calbet, J.C. Grenier, A. Waittiaux, P. Hagenmuller, J. Solid State Chem. 46 (1983) 23.
[38] S. García-Martín, M.Á. Alario-Franco, H. Ehrenberg, U. Amador, J. Am. Chem. Soc. 126 (2004) 3587.
[39] A. Martinelli, C. Artini, M.R. Cimberle, G.A. Costa, M. Ferreti, R. Masini, P. Mele, Phys. Rev. B 69 (2004) 052507.
[40] O.I. Lebedev, G. Van Tendeloo, G. Cristiani, H.U. Habermeier, A.T. Matveev, Phys. Rev. B 71 (2005) 134523.
[41] O.I. Lebedev, G. Van Tendeloo, J.P. Attfield, A.C. McLaughlin, Phys. Rev. B 73 (2006) 224524.
[42] A.G. Fitzgerald, M. Mannami, Proc. R. Soc. A 293 (1966) 169.
[43] M.Á. Alario-Franco, Cryst. Latt. Def. Amorph. Mater. 14 (1987) 357.
[44] W. Massa, in: second ed.W. Massa (Ed.), Crystal Structure Determination, vol. 1, Springer, Berlin, 2004, p. 129 (Chapter 10).
[45] A. Werner, H.D. Hochheimer, Phys. Rev. B 25 (1982) 5929.
[46] L.C. Bourne, P.Y. Yu, A. Zettl, L. Marvin Cohen, Phys. Rev. B 40 (1989) 10973.
[47] A.J. Dos santos-García, G. Heymann, H. Huppertz, M.Á. Alario-Franco, Turning points in solid-state, materials and surface chemistry: "High pressure and high temperature oxidation in the $IrSr_2RECu_2O_8$ family of cuprates: The disordered multiple perovskite $(A_{1/3}\,A'_{2/3})(B_{1/3}\,B'_{2/3})O_{3-x}$ phases," in: K.D.M. Harris, P.P. Edwards (Eds.), Royal Society of Chemistry Edited Text, RSC Publishing, Cambridge, 2007, p. 151 (Chapter 9).
[48] S.A. Grigera, R.S. Perry, A.J. Schofield, M. Chiao, S.R. Julian, G.G. Lonzarich, S.I. Ikeda, Y. Maeno, A.J. Millis, A.P. Mackencie, Science 294 (2001) 329.
[49] R.S. Perry, L.M. Galvin, S.A. Grigera, L. Capogna, A.J. Schofield, A.P. Mackenzie, M. Chiao, S.R. Julian, S.I. Ikeda, S. Nakatsuji, Y. Maeno, C. Pfleiderer, Phys. Rev. Lett. 86 (2001) 2661.
[50] A.J. Millis, A.J. Schofield, G.G. Lozarich, S.A. Grigera, Phys. Rev. Lett. 88 (2002) 217204.
[51] J.G. Zoltán, O.J. Rutt, C.F. Smura, T.P. Overton, N. Barrier, S.J. Clarke, J. Hadermman, J. Am. Chem. Soc 128 (2006) 8530.
[52] I.S. Jacobs, P.E. Lawrence, Phys. Rev. 164 (1967) 866.
[53] I. Felner, V.P.S. Awana, E. Takayama-Muromachi, Phys. Rev. B 68 (2003) 094508.
[54] J.R. Luo, N.L. Wang, G.T. Liu, D. Wu, X.N. Jing, F. Hu, T. Xiang, Phys. Rev. Lett. 93 (2004) 187203.